

# Multi-energy four-channel Kirkpatrick–Baez microscope for X-ray imaging diagnostics at the Shenguang-II laser facility

Shengzhen Yi (伊圣振)<sup>1,2,3</sup>, Baozhong Mu (穆宝忠)<sup>1,2,\*</sup>, Xin Wang (王新)<sup>1,2</sup>,  
Li Jiang (蒋励)<sup>1,2</sup>, Jingtao Zhu (朱京涛)<sup>1,2</sup>, Zhanshan Wang (王占山)<sup>1,2\*\*</sup>,  
Pengfei He (贺鹏飞)<sup>1,3</sup>, Zhiheng Fang (方智恒)<sup>4</sup>, Wei Wang (王伟)<sup>4</sup>,  
and Sizu Fu (傅思祖)<sup>4</sup>

<sup>1</sup>MOE Key Laboratory of Advanced Micro-Structured Materials, Shanghai 200092, China

<sup>2</sup>School of Physics Sciences and Engineering, Tongji University, Shanghai 200092, China

<sup>3</sup>School of Aerospace Engineering and Applied Mechanics, Tongji University,  
Shanghai 200092, China

<sup>4</sup>Shanghai Institute of Laser Plasma, CAEP, Shanghai 201800, China

\*Corresponding author: mubz@tongji.edu.cn; \*\*corresponding author: wangzs@tongji.edu.cn

Received April 14, 2014; accepted June 3, 2014; posted online August 23, 2014

A four-channel Kirkpatrick–Baez microscope working at multiple energy bands is developed for multiframe X-ray imaging diagnostics at the Shenguang-II laser facility. The response to the multiple energy bands is realized by coating the double-periodic multilayers on the reflected surfaces of the microscope. Because of the limited size of the microstrips in the X-ray framing camera, the image separation is controlled by the conical angle of the reference cores during microscope assembly. This study describes the optical and multilayer design, assembly, and alignment of the developed microscope. The microscope achieves a spatial resolution of 4–5  $\mu\text{m}$  in the laboratory and 10–20  $\mu\text{m}$  at Shenguang-II laser facility within a 300  $\mu\text{m}$  field of view. The versatile nature of the developed microscope enables the multiple microscopes currently installed in the laser facility to be replaced with a single, multipurpose microscope.

OCIS codes: 340.7440, 310.6845, 340.7470.

doi: 10.3788/COL201412.093401.

X-ray multiframe imaging is an important method in plasma diagnostics of laser inertial confinement fusion (ICF). The detailed spatial and temporal evolution of plasma density and temperature can be analyzed by multiframe imaging of X-ray line emission passed through imploded ICF targets (in radiography mode) or radiated from the trace layer (in self-imaging mode). The Kirkpatrick–Baez (KB) microscope provides higher spatial resolution (3–5  $\mu\text{m}$  within field of view (FOV) of several hundred micrometers) and a collecting solid angle ( $\sim 10^{-7}$  sr) larger than X-ray pinhole arrays<sup>[1,2]</sup>. Coupled to a framing camera, KB microscope enables observation of precise physical processes, such as hydrodynamic instabilities and evolution of distortions in the imploding ICF target, at high-power laser facilities<sup>[3–5]</sup>.

By coating the metal single layer or X-ray multilayers on the reflected surfaces, the KB microscopes were specifically designed to operate at different energy bands to meet a range of diagnostic needs. The metal single layers (e.g., Ir or Pt) based on total external reflection are good elements to use in the soft X-ray region, such as 1.25 keV (U N-band) for X-ray backlighters<sup>[2,6,7]</sup> and 2.79 keV (Cl He-like Ly  $\alpha$ ) for X-ray self-emission<sup>[8]</sup>. KB microscopes whose reflecting surfaces are coated with single layer can also respond to harder X-rays, but only at grazing angles smaller than the critical angle of total ex-

ternal reflection, which limits the spatial resolution. The multilayer coatings consisting of alternating bilayers of high- and low-Z materials are a good solution to achieve a large grazing angle with a narrow high-throughput bandpass. This can be understood by the Bragg diffraction formula  $2D\sin\theta = m\lambda$ <sup>[5,9]</sup>, where  $D$  is the periodic thickness of the multilayers,  $\theta$  is the grazing angle,  $m$  is the order of X-ray diffraction, and  $\lambda$  is the X-ray wavelength. Such X-ray multilayers are designed to work at a given energy band; for instance, 4.95 keV (V K $\alpha$ ) or 8.05 keV (Cu K $\alpha$ ), used for X-ray backlighters<sup>[10,11]</sup>.

To meet the various energy requirements of diagnostic experiments, such as Rayleigh–Taylor (RT) growth measurement by Cu L-band (1.0–1.3 keV) or U N-band (1.25 keV) backlighter, implosion trajectory measurement by Mo L-band (2.3–2.6 keV) or Ag L-band (3.2–3.6 keV) backlighter<sup>[12]</sup>, and electron transport measurement by Cu K $\alpha$  (8.05 keV) X-ray imaging<sup>[13]</sup>, we develop a four-channel KB microscope that responds to multiple energy bands and is applicable to various time-gated X-ray imaging diagnostics on Shenguang-II (SG-II). The optical and multilayer design, assembly, and alignment method, and experimental evaluation of the microscope are described below.

The design of the four-channel KB microscope has been previously published<sup>[2,7]</sup>; therefore, the selection of

the geometric parameters is not discussed here. The final optical parameters of the microscope are listed in Table 1. To achieve the desired reflectivity in the 8.05 keV energy band, the selected grazing incidence angle  $\theta$  is set to approximately  $1^\circ$  although a larger value can be used if only working at the soft X-ray region. The magnifications were approximately  $8\times$  to achieve sufficient brightness at the image plane. In ZEMAX (Radiant Zemax, USA) simulations, the spatial resolution of the microscope was found to near-linearly decrease from  $2\ \mu\text{m}$  in the central FOV to almost  $5\ \mu\text{m}$  within a FOV of  $300\ \mu\text{m}$ . Under the magnification of about  $8\times$ , the actual spatial resolution will be limited by the pixel size of framing camera ( $30 \times 30\ (\mu\text{m})$ ), but it is still enough to satisfy the current requirements of SG-II diagnostics experiments such as  $50\ \mu\text{m}$  wavelength RT growth-rate measurement.

To enable response to multiple X-ray energy bands, the reflecting surfaces of the KB mirrors are coated with a type of multilayers with two stacks, as shown in Fig. 1. The top and bottom stacks (with the same grazing angle but different period thicknesses) are designed to respond to different X-ray energy bands. Soft x-rays with short penetration depth are directly reflected by the top stack. Harder X-rays (8.05 keV in this study, corresponding to the Cu  $K\alpha$  line) can penetrate more deeply into the multilayers than soft X-rays, they are of enough intensity after passing through the top and then be reflected by the bottom stack.

The top and bottom stacks of our developed microscope are constructed from Cr/C and W/Si multilayers, respectively. The Cr/C multilayers comprise two bilayers (period thickness = 21.27 nm; thickness ratio = 0.316), while the W/Si multilayers comprise 25 bilayers (period thickness = 4.79 nm; thickness ratio = 0.600). The grazing angle of both stacks is  $1.000^\circ$ . At the larger grazing angle ( $1.045^\circ$ ), the Cr/C multilayers comprise two bilayers (period thickness = 21.73 nm; thickness ratio = 0.321) and the W/Si multilayers comprise 25 bilayers (periodic thickness = 4.61nm; thickness ratio = 0.573). Figure 2 shows the calculated spectral response of the multilayers subtended by two reflections at grazing angles of  $1.000^\circ$  and  $1.045^\circ$ , which correspond to the central FOV. X-ray energy below 2 keV responds due to total external reflection by the Cr in the top layer. In this energy range, the microscope can be used for RT growth measurement by Cu L-band (1.0–1.3 keV) or U N-band (1.25 keV) backlighter. At the thickness ratio of 0.316,

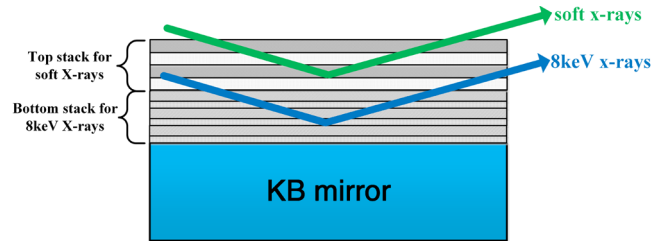


Fig. 1. Schematic of double-periodic multilayers and their effect on X-ray energy bands.

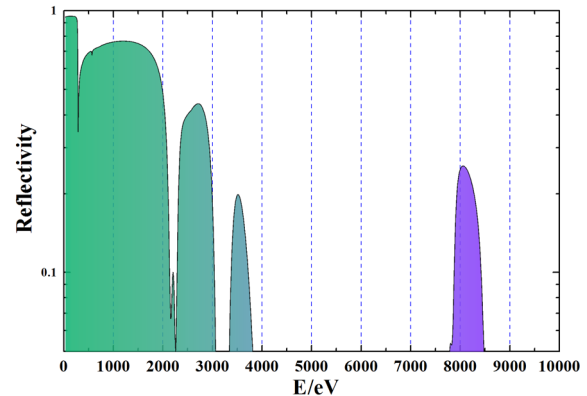


Fig. 2. Calculated spectral response of Cr/C and W/Si double-periodic multilayers at the central FOV, subtended by two reflections in the tangential and sagittal directions.

the top Cr/C multilayers stack was tuned to simultaneously respond to two soft X-ray energy bands, 2.6 and 3.5 keV. These energy bands can be used for implosion trajectory measurement by Mo L-band (2.3–2.6 keV) or Ag L-band (3.2–3.6 keV) backlighter. The 8.05 keV energy band is responded by W/Si multilayers stack, and can be used for electron transport measurement by Cu  $K\alpha$  (8.05 keV) X-ray imaging. The microscope can also be used for imaging of the bremsstrahlung radiation (at multi-keV X-ray energy bands) from the imploded target by spectrum selection of different filters in the four channels.

It should be noted that the top Cr/C bilayer stack will reduce the reflectivity of the bottom W/Si multilayer stack for Cu  $K\alpha$  line. For  $\theta = 1.0^\circ$  design, the theoretical reflectivity of Cu  $K\alpha$  line decreases from 73.7% to 54.2%, that is, 73.5% hard X-ray penetrates into Cr/C stack. For  $\theta = 1.045^\circ$  design, the theoretical reflectivity of Cu  $K\alpha$  line decreases from 72.7% to

**Table 1.** Optical Parameters of Four-channel KB Microscope

Direction	R (m)	M	$\theta$ (deg.)	u (mm)	v (mm)	d (mm)
Tangential ( <i>t</i> )	19.5	8.00	1.000	191.4	1531.2	10
Sagittal ( <i>s</i> )	19.5	7.55	1.045	201.4	1521.2	10

*R* is the curvature radius of KB mirrors, measured by an optical profiler (Contour GT-X3, Bruker, USA), *M* is the magnification of the KB microscope,  $\theta$  is the grazing incidence angle of KB mirrors for central FOV, *u* is the object distance of KB mirrors, *v* is the image distance of KB mirrors, and *d* is the length of KB mirrors along the optical axis.

51.6%. So, more than 70% hard X-ray can penetrate into Cr/C stack to provide significant Cu  $K\alpha$  line intensity. Another challenge to deposit this double-periodic multilayer is the strain problem. Before combining two stacks, Cr/C and W/Si stacks were deposited, respectively, and their strain effect was studied. The ratio of layer thicknesses was optimized to balance the strain into multilayer. Then, the strain experiment was performed again after combination of two stacks onto KB mirrors. No strain problem on the overall performance of the KB mirror was found in our experiment.

Consequent to serious off-axis aberration, the spatial resolution of the KB microscope decreases with deviation from the central FOV. The four-channel KB microscope shown in Fig. 3(a) includes four concave spherical mirrors stacked in two perpendicular pairs, forming four images of the ICF target. To coincide the central FOVs (with best spatial resolution) of all four channels at the same target position, high-precision assembly is required. Furthermore, the four images must be separated by specific distances to couple to the microstrips of the framing camera. The accurate assembly of our developed microscope was also realized by the method of conical reference cones as shown in Fig. 3 (with a detailed description in Yi *et al.*<sup>[14]</sup>). The method uses the reference cone with a conical angle  $\alpha$  to accurately control the image separations ( $2L$ ) at a specified value to couple to the microstrips of the framing camera. The existing framing camera is fitted with three microstrips separated by 10.8 mm, of which the first and third microstrips (i.e.,  $2L = 21.6$  mm) are intended for use in our design. According to the optical parameters listed in Table 1, the sizes of the conical reference cones can be determined from the thickness  $(2y)_1 = 9.404$  mm and conical angle  $\alpha_1 = 0.419^\circ$  in the tangential direction, and from  $(2y)_2 = 10.378$  mm and  $\alpha_2 = 0.442^\circ$  in the sagittal direction.

Because visible wavelengths are highly diffracted, the four-channel KB microscope must be accurately aligned in an X-ray imaging experiment of the metal grid. In the alignment procedure conducted in this study, the calibration image was a 600-mesh Au grid (41  $\mu\text{m}$  period with approximately 6  $\mu\text{m}$  linewidth, measured by

scanning electron microscopy (SEM)), backlit by a copper X-ray tube (8.05 keV) operating at 38 kV voltage and 20 mA current. A phosphor X-ray charge coupled device (CCD) camera (Photonic Science: XDI-50) with  $696 \times 520$  pixels (corresponding to  $12.9 \times 12.9$  ( $\mu\text{m}$ )) was affixed to a motorized  $x$ - $y$ - $z$  axis translation stage and placed on the image plane. Four KB mirrors were pressed onto two conical reference cones by ball plungers, and were then aligned in the tangential and sagittal directions. Figure 4 shows X-ray images of the Au grid imaged by the microscope in the laboratory. The X-ray CCD was shifted to cover four images separated by 21.6 mm under the control of the translation stage. The 120  $\mu\text{m}$  hole punctured in the grid serves as a positional reference from the object to the image. Comparing the grid period imaged by the CCD with the SEM-calibrated image, the magnifications are approximately 8.4 and 7.9 in the horizontal (tangential) and vertical (sagittal) directions, respectively. The grid wires (approximate width 6  $\mu\text{m}$ ) are stark near the reference hole, and gradually blur out with increasing FOV. On the basis of the 10%–90% criterion<sup>[15]</sup>, the measured spatial resolution of our microscope ranges from 4 to 5  $\mu\text{m}$  in the horizontal direction of positions (a)–(d).

In switching from the X-ray laboratory to SG-II deployment, we identified the best FOV using a 500  $\mu\text{m}$ -diameter removable ball pointer. The ball pointer was connected to a high-precision industrial linear guide (HIWIN, MGN15H)<sup>[16]</sup> affixed to the microscope. The ball pointer could be removed from the linear guide and the positioning accuracy could be repeated up to 20  $\mu\text{m}$ . Meanwhile, the center of the four image points was indicated by a red diode laser ( $\Phi \sim 1$  mm), also affixed to the microscope. The alignment process in the SG-II chamber was instructed by the target viewing system. The microscope was aligned by an  $x$ - $y$ - $z$  translation stage until the ball pointer was positioned at the target center. The X-ray framing camera was centralized at the position indicated by red diode laser. Finally, the ball pointer and red diode laser were removed from the microscope, and the chamber was vacuum-pumped.

The final spatial resolution of the microscope coupled to the framing camera was tested in X-ray imaging experiments. The test target was a four-quadrant grid (150/200/300/400 mesh) with 10  $\mu\text{m}$  linewidth. The reference ball pointer was centralized at the coordinate origin of the grid. The debris filter was a beryllium foil (thickness = 20  $\mu\text{m}$ ) positioned prior to the microscope. The backlighters (Cu and Mo foils) were separately irradiated by two shots of the ninth beam of SG-II (2 ns,  $3w$ , 1 kJ). The grid was imaged at four different times by the framing camera (FOV =  $1340 \times 1300$  pixels, pixel size  $30 \times 30$  ( $\mu\text{m}$ ), MCP diameter  $\Phi = 36$  mm), as shown in Fig. 5. The experiment results shown in Figs. 4 and 5 demonstrated the ability of our developed microscope to work at multiple X-ray energy bands. The changing image brightness in the four channels

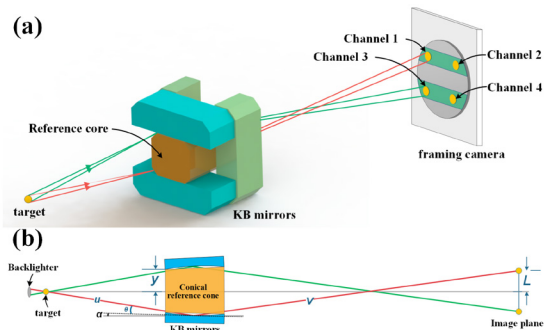


Fig. 3. (a) Schematic of the four-channel KB microscope and (b) imaging in the tangential direction. The image separation ( $2L$ ) is accurately controlled by the conical angle  $\alpha$ .

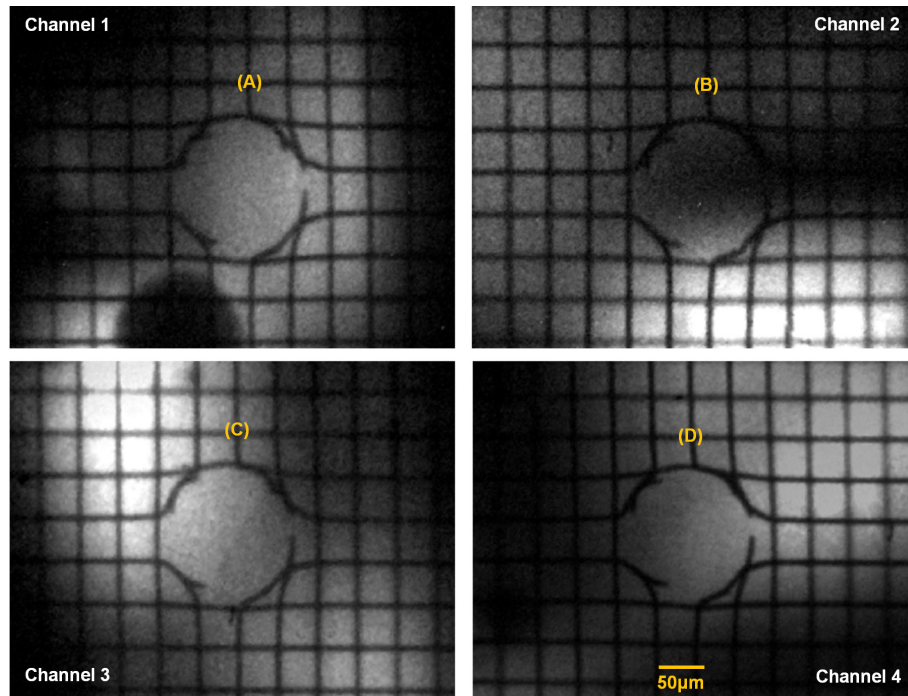


Fig. 4. Images of 600-mesh Au grid acquired by a phosphor X-ray CCD with an exposure time of 30 min. The grid (approximate linewidth =  $6\ \mu\text{m}$ ) was illuminated by a copper X-ray tube (8.05 keV). The X-ray CCD was shifted to cover four images separated by 21.6 mm. The shift was controlled by a motorized  $x$ - $y$ - $z$  axis translation stage.

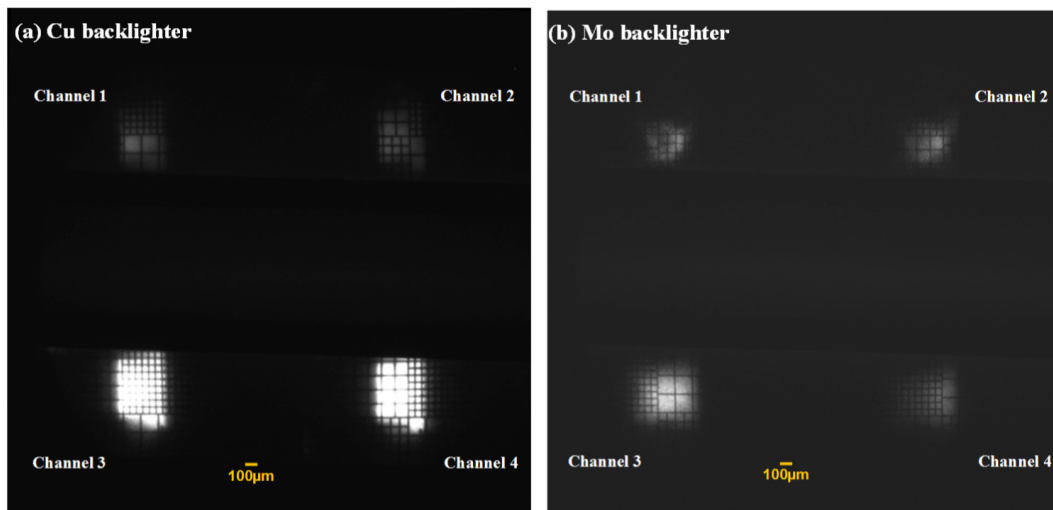


Fig. 5. Testing the spatial resolution of the microscope: images of a four-quadrant Au grid (150/200/300/400 mesh) were acquired by the framing camera. The images were located on the first and third microstrips of the framing camera. The grid (approximate linewidth =  $10\ \mu\text{m}$ ) was illuminated by 1.0–1.3 keV (Cu L-band, left image) and by 2.3–2.6 keV backlighters (Mo L-band, right image). The response ability to 8.05 keV has been demonstrated by the X-ray imaging experiments in the laboratory with the results shown in Fig. 4.

reflects the fluctuating laser intensity, and is lower in Fig. 5(b) than in Fig. 5(a) because of the lower yield of the X-rays generated by the Mo backlighter. Since the optical axis of each channel occurs at a different position of the backlighter (see Fig. 3(b)), the backlighter center is offset from the coordinate origin of the grid.

The final spatial resolution of the microscope on SG-II is degraded to some extent by the limited pixel size of the framing camera ( $30 \times 30\ (\mu\text{m})$ ). For example, in

channel 2 (see Fig. 5(a)), the measured spatial resolution, based on the 10%–90% criterion, is approximately  $10\ \mu\text{m}$  near the coordinate origin and better than  $20\ \mu\text{m}$  within the  $300\ \mu\text{m}$  FOV, as plotted in Fig. 6. The image separation between the four channels was also accurately calibrated to approximately  $709 \times 702$  pixels in the horizontal and vertical directions, respectively, corresponding to respective real separations of  $21.3 \times 21.1$  (mm), very close to the design values of  $21.6 \times 21.6$  (mm).

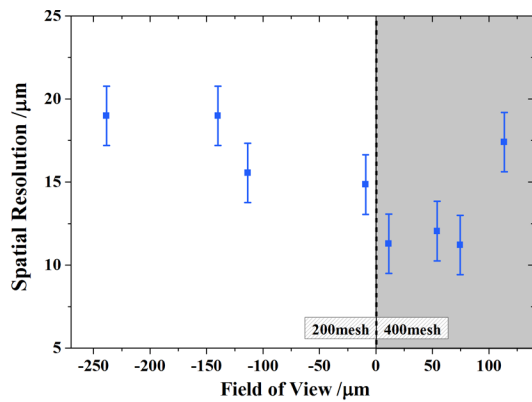


Fig. 6. Spatial resolution calibration of channel 2 in Fig. 5(a). The resolution is approximately  $10\ \mu\text{m}$  in the central FOV and better than  $20\ \mu\text{m}$  within the  $300\ \mu\text{m}$  FOV. Error bars correspond to the width of one pixel ( $30\ \mu\text{m}$ ) divided by the magnification ( $8.4\times$ ).

We successfully develop a four-channel KB microscope that operates in multiple X-ray energy bands. The microscope is intended for use in plasma diagnostics on SG-II. The response to multiple energy bands is realized by coating the reflecting surfaces of the microscope with double-periodic multilayers. A test grid is imaged in the laboratory and on SG-II to a spatial resolution of  $4\text{--}5$  and  $10\text{--}20\ \mu\text{m}$ , respectively, within a  $300\ \mu\text{m}$  FOV. The microscope images multiframe X-ray line emission on SG-II in radiography or self-emission mode, and is applicable to various diagnostic experiments requiring different X-ray energies.

The high-voltage pulse of the framing camera propagates at a fixed velocity (nearly half the speed of light). Consequently, the time interval between two images on the same microstrip is limited to approximately  $140\ \text{ps}$  at an image separation of  $21.6\ \text{mm}$ , and only two brief time segments are captured on two microstrips, which is insufficient to cover the evolution of laser plasma. To correct this problem, we rearrange the four images on the microstrips of the framing camera, as shown in Fig. 7. The redesigned image separations can be controlled to  $20.0 \times 23.1\ (\text{mm})$  using the assembly method with conical reference cones. The four microstrips are separated by  $10\ \text{mm}$  and rotated  $30^\circ$  along the symmetric axis. The images of the four-channel KB microscope are then coincident with the four microstrips of the framing camera, and be gated on four different times by changing delay times between individual microstrips. The spatial resolution can be further improved by increasing the magnification of the microscope.

This work was supported by the National Natural Science Foundation of China (Nos. 11305116 and 11105098), the National Key Technology Support

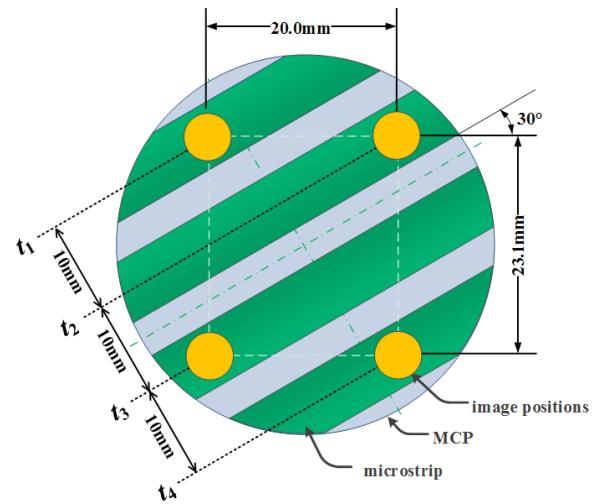


Fig. 7. Redesigned arrangement of four images onto the microstrips of the framing camera.

Program of China (No. 2013BAK14B02), and the National “973” Program of China (No. 2011CB922203).

## References

1. P. Kirkpatrick and A. V. Baez, *J. Opt. Soc. Am.* **38**, 766 (1948).
2. F. J. Marshall and Q. Su, *Rev. Sci. Instrum.* **66**, 725 (1995).
3. F. J. Marshall, *Rev. Sci. Instrum.* **83**, 10E518 (2012).
4. R. Rosch, J. Y. Boutin, J. P. le Breton, D. Gontier, J. P. Jadaud, C. Reverdin, G. Soullie, G. Lidove, and R. Maroni, *Rev. Sci. Instrum.* **78**, 033704 (2007).
5. T. Pardini, T. J. McCarville, C. C. Walton, T. A. Decker, J. K. Vogel, P. B. Mirkarimi, J. B. Alameda, R. M. Hill, L. A. Pickworth, V. A. Smalyuk, J. M. Ayers, P. M. Bell, D. K. Bradley, J. D. Kilkeny, and M. J. Pivovarov, *Proc. SPIE* **8850**, 88500E (2013).
6. O. V. Gotchev, L. J. Hayes, P. A. Jaanimagi, J. P. Knauer, F. J. Marshall, and D. D. Meyerhofer, *Rev. Sci. Instrum.* **74**, 5065 (2003).
7. F. J. Marshall, M. M. Allen, J. P. Knauer, J. A. Oertel, and T. Archuleta, *Phys. Plasmas* **5**, 1118 (1998).
8. F. J. Marshall and J. A. Oertel, *Rev. Sci. Instrum.* **68**, 735 (1997).
9. J. H. Underwood, *Rev. Sci. Instrum.* **57**, 2119 (1986).
10. O. V. Gotchev, P. A. Jaanimagi, J. P. Knauer, F. J. Marshall, and D. D. Meyerhofer, *Rev. Sci. Instrum.* **75**, 4063 (2004).
11. F. J. Marshall and G. R. Bennett, *Rev. Sci. Instrum.* **70**, 617 (1999).
12. J. J. Dong, Z. R. Cao, Z. H. Yang, B. L. Chen, T. X. Huang, B. Deng, S. Y. Liu, S. E. Jiang, Y. K. Ding, S. Z. Yi, and B. Z. Mu, *Acta Phys. Sin.* **61**, 155208 (2012).
13. H. Friesen, H. F. Tiedje, D. S. Hey, M. Z. Mo, A. Beaudry, R. Fedosejevs, Y. Y. Tsui, A. Mackinnon, H. S. McLean, and P. K. Patel, *Rev. Sci. Instrum.* **84**, 023704 (2013).
14. S. Yi, B. Mu, X. Wang, J. Zhu, L. Jiang, Z. Wang, and P. He, *Chin. Opt. Lett.* **12**, 013401 (2014).
15. S. W. Smith, *The Scientist and Engineer's Guide to Digital Signal Processing* (California Technical Publishing, San Diego, 1997) pp. 423
16. HIWIN Corporation, Linear Guideway Technical Information, [http://www.hiwin.com/html/extras/mgn-c\\_mgn-h.html](http://www.hiwin.com/html/extras/mgn-c_mgn-h.html) (2014).